Pereira, JC.; Zambrano, JC.; Rayón, E.; Yañez, A.; Amigó, V. (2018). Mechanical and microstructural characterization of MCrAlY coatings produced by laser cladding: The influence of the Ni, Co and Al content. Surface and Coatings Technology. 338:22-31. https://doi.org/10.1016/j.surfcoat.2018.01.073

Mechanical and microstructural characterization of MCrAlY coatings produced by laser cladding. The influence of the Ni, Co and Al content

J. C. Pereira [1] *, J. C. Zambrano [2], E. Rayón [2], A. Yañez [3], V. Amigó [2]

[1] IK4-Lortek, Arranomendia, 4A, 20240 Ordizia, Gipuskoa, Spain.
[2] Institute of Materials Technology (ITM), Universitat Politècnica de Valencia, camino de vera s/n, 46022. Spain.
[3] Laboratorio de Aplicaciones Industriales del Láser. Centro de Investigaciones Tecnológicas. Universidade da Coruña. 15403 Ferrol, Spain.
* jcpereira@lortek.es *phone: +34 943 882 303 fax: +34 943 884 345*

Abstract

Laser metal deposition (LMD) and laser cladding (LC) are alternative methods to thermal spraying processes to produce dense, high-quality coats. In this work, two MCrAlY coatings (M=Ni+Co) have been prepared onto stainless substrate using a coaxial LC technique under two different Ni/Co and Al proportions. The mechanical properties were then evaluated with microhardness, nanoindentation, and three-point bending tests. The microstructure and composition of coatings were characterized by X-Ray Diffraction (XRD) analysis and Field Emission Electron Microscopy (FESEM) coupled to an Energy Dispersive Spectroscopy (EDS) detector. The study revealed that the γ/β phases formed in the MCrAlY coating microstructure result in a lower elastic modulus than the austenitic stainless steel substrate, while an inverse behavior for hardness was observed due the presence of the aluminum-rich β-phase. Under flexural loads, the failure of coatings showed plasticity and anisotropy characteristics depending on the two laser tracks orientations evaluated.

Keywords: MCrAlY; laser cladding; nanoindentation; hardness; elastic modulus; ductility.

1. Introduction

Aircraft and power-generation turbines are made from metallic components that are protected by thermal barrier coatings (TBCs). A TBC system is usually formed by a top ceramic layer [1,2] deposited onto a bond layer [3,4] over the substrate. The materials widely used for bond

coatings are composed of MCrAlY superalloys (where M=Ni, Co, Fe or combinations of these). NiCoCrAlY and CoNiCrAlY are the most common superalloys used as bond coats [5] due to their good adhesion, optimal elastic modulus, high strength, and high-temperature oxidation [6]. These MCrAlY alloys usually contain large amounts of Cr with small additions of Y, which hardens the solid solution. This solid solution effect of these elements blocks the dislocation movements through the grain boundaries, enhancing the common creep resistance of MCrAlY alloys [7]. Otherwise, an Al content between 8-15 wt% slows down crystal growth, resulting in a more thermally stable, adherent and continuous aluminum-rich oxide layer (α-Al_2O_3) [8,9]. Furthermore, it increases the amount of β-(Ni,Co)Al phase, which is harder than the gamma matrix phase in γ/β MCrAlY coatings [10].

Nowadays, the laser cladding process (LC) is gaining attention as an alternative technique to manufacture TBC coatings. Laser cladding can be applied as a rapid manufacturing technique consisting of the direct deposition of metallic alloys with high melting points, such as MCrAlY alloys. Specifically, coaxial laser cladding uses a special nozzle head to create a coniform annular gap, which encircles the focused laser beam with powder, melting the powder on the surface to be coated. The coaxial LC process has been tested to produce large, dense coatings by overlapping single laser tracks [11,12]. Even complex 3D pieces are able to be coated by LC using powder or solid wire as a material feedstock. In the same way, laser metal deposition (LMD) processes use this principle to deposit the material layer by layer in an innovative additive manufacturing process [13–15]. The continuous coatings obtained by these techniques are free of pores and cracks when the experimental conditions are well-controlled. These properties improve the resultant mechanical resistance and interfacial strength with the substrate. However, due to the brittle behavior of MCrAlY alloys at low temperatures [16], the experimental conditions must be well-studied and controlled in order to avoid residual stresses and material defects (pores, cracks, lack of fusion, and others) [17,18]. Furthermore, several studies [19] have reported that the diffusion zone achieved between the

coating and substrate is critical to optimize the resultant mechanical properties, it being desirable to reduce the chemical dilution of the coating to substrate. Moreover, the elastic modulus of the bond coat is also a critical mechanical parameter, since TBC systems are composed of several layers. The shear stresses expected between layers must be as low as possible to avoid delamination failures [5,6].

In this study, two MCrAlY coatings have been produced by the coaxial LC process. One coat was made with a higher concentration of Ni and Al, called NiCoCrAlY. The other was prepared with a higher concentration of Co, called CoNiCrAlY, for comparative purposes. After finding the best experimental conditions to form dense, continuous coatings using pre-alloyed powder as a feedstock material, an in-depth mechanical characterization was performed. In order to complete the study, the elastic modulus and hardness of the individual phases and of the whole coating were evaluated by nanoindentation [10,20–22]. Also, to analyze the strength and fracture mechanisms of the interface between layers, a three-point bending test was used [23,24]. Besides these techniques, other properties were investigated through measurements of microhardness and microstructural analysis by XRD, FESEM and EDS.

2. Experimental procedure

2.1 Materials and processing techniques

The feedstock materials used in this study were two commercial MCrAlY pre-alloyed powders supplied by Oerlikon Metco. A Ni-rich powder called NiCoCrAlY (Amdry 365-2) was mainly composed of (wt.%) 47.1% Ni, 23% Co, 17% Cr, 12.5% Al and 0.4% Y. The mean particle size diameter was given by the supplier as 55 µm. In addition, a Co-rich powder called CoNiCrAlY (Amdry 995C) and composed of 38% Co with 32% Ni, 21% Cr, 8% Al and 0.45% Y was used to produce the second coating, with a mean particle size diameter of 65 µm. The substrate was a cold-rolled austenitic stainless steel sheet (AISI 304) with a thickness of 10 mm. Extensive coatings (30x30 mm^2) were obtained using a Nd:YAG solid

state laser (Rofin-Sinar DY 022) in continuous mode and λ=1064 nm. The laser power was programmed at 2.2 kW (maximum power). The diameter of the beam spot onto the substrate surface was 4 mm. The XYZ movement was achieved with a robotic-arm (ABB IRB 2400 unit) with 6 degrees of freedom. The scan velocity was set to 15 mm/s and the overlap ratio between tracks was programed to reach 40%. The powder was gas-assisted at a rate of 25 mg/mm using a coaxial annular nozzle (Precitec YC50) and a Sulzer Metco Twin 10-C powder feeder. Helium was used as a shielding and powder carrier gas, flowing at 20 l/min.

2.2 Coating characterization and microstructure

The microstructural characterization of the coating and substrate was analyzed on a cross-sectional view. Samples were cut and metallographically prepared using diamond abrasives of different grits. The compositional analysis was determined using a backscattered electron image detector (BSE) and energy dispersive spectroscopy (EDS) coupled inside a field emission scanning electron microscope (FESEM) (Zeiss ULTRA55). The crystalline characterization of the main phases was performed by X-ray diffraction (XRD) using a Philips X'pert diffractometer with monochromatic Cu-K_α radiation (λ=0.15406 nm). The XRD patterns were obtained in the 2θ range from 20° to 90° and were subsequently analyzed using the X'Pert Plus software (PANalytical).

2.3 Mechanical tests

Three different tests were used for the mechanical characterization of the produced coatings and their individual phases and microstructures.

2.3.1. Microhardness measurements

Vickers hardness profiles from the coating surface to the substrate were evaluated in cross-sections by a microhardness tester (Shimadzu HMV-2, Japan) assisted by automatic measurement software. Three indentation arrays were replicated for each coating, spaced 100 μm apart. Results were subsequently averaged to obtain the microhardness profile for each

coat. All tests were performed under a constant 980.7 mN load ($HV_{0.1}$) for 10 seconds, following the standard guidelines described by ASTM E384 [25].

2.3.2. Elastic modulus and nanohardness measurements

In order to obtain the elastic modulus and nanohardness of the whole coatings and main microstructural phases, a G-200 nanoindenter from Agilent Nanotech was used. Tests were performed under continuous stiffness measurement mode (CSM) in order to acquire the in-depth stiffness profiles. A matrix of 25 indentations was performed on the cross-section of each coating at a constant 2000 nm depth with displacement control, and the corresponding variation of force as a function of displacement was continuously recorded. From the measured data and following the method of *Oliver and Pharr* [26], the hardness *H* and the elasticity modulus *E* were calculated. Subsequently, the depth range used to calculate the characteristics of the single phases was evaluated through the observation and analysis of the acquired curves. In this way, we can ensure that the calculated hardness and elastic modulus values correspond to individual phases [4,27]. The Poisson's coefficient used for the Young's Modulus calculation was 0.3 for all tests.

2.3.3. Three-point bending test measurements

Three-point bending tests were performed on the coating-substrate system and in the substrate sample. A universal test machine (Shimadzu model AG-X, Japan) with a 50 kN load-cell and camcorder extensometry was used. The bending device was configured by three hardened steel rollers with 5 mm radius (Fig. 1). The distance between rollers was adjusted to 22 mm according to the thickness of the samples (coating + substrate). The deflection on the outer surface of the coating was measured during the test by an Epsilon Technology digital deflectometer, model 3540-004M-ST. The movement of the punch during the test was simultaneously recorded. The speed was 0.50 mm/min at a constant displacement control.

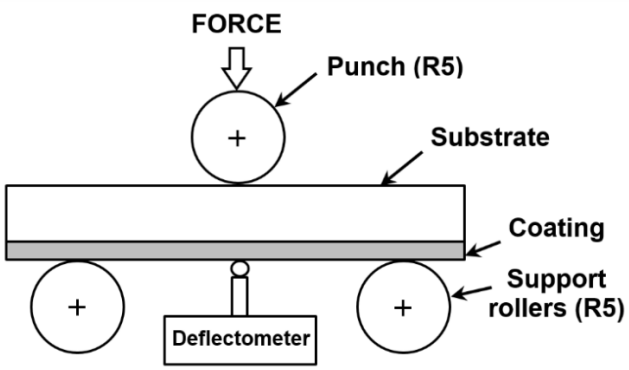

Fig. 1 Schematic of the three-point bending test configuration

The load versus displacement curve was recorded, as well as the load curve vs. central deflection at the coating surface (mm), and from these data the bending nominal stress ($\sigma_{flexion}$) and the strain (ε_{ext}) of the outer fiber (coating surface) were calculated using equations 1 and 2, respectively.

$$\sigma_{flexion} = \frac{3.L.F}{2.b.t^2} \quad \text{(Eq. 1)}$$

$$\varepsilon_{ext} = \frac{6.t.d}{L^2} \quad \text{(Eq. 2)}$$

Where L is the distance between the lower rollers, F is the applied centered load, b is the sample width, t is the total thickness of the sample (substrate + coating) and d is the deflection measured at the centerline of the outer coating surface by the digital deflectometer. From the stress-strain curve, the flexural elastic modulus, the yield strength (0.2% of the deformation method), and the rupture stress (the stress that provokes cracks or detachment of coating from substrate) were calculated. For the coating/substrate system, three samples were cut in two different orientations (transverse and longitudinal to the laser tracks direction) with resultant dimensions of 30x8x3.8 mm (Fig. 2).

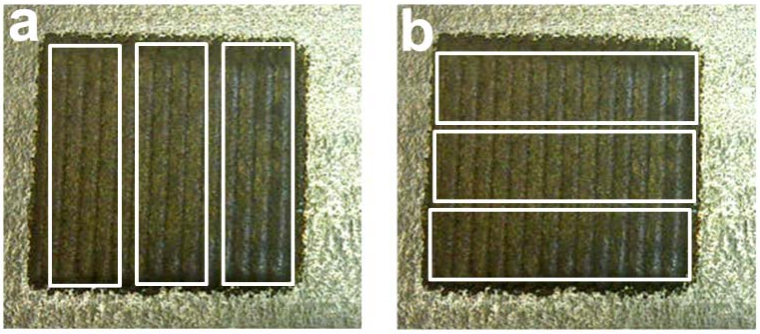

Fig. 2 Schematic of sample cutting for bending tests **a)** Longitudinal and **b)** Transverse

3. Results and discussion

3.1 MCrAlY laser cladding coatings and their microstructure

Many variables are involved in the coaxial laser cladding process, requiring a previous study to find the optimal experimental conditions. In previous works published by the authors [28–30], the parameters for coaxial laser cladding were studied to obtain MCrAlY coatings with an adequate aspect ratio, homogeneity, low chemical dilution and a good metallurgical bonding with the substrate [31]. The high velocity, powder feed rate and laser power were also selected to improve the efficiency of the process (high deposition rate and low powder loss), resulting in a faster process. The specific laser energy (36.67 J/mm^2) combined with a 4 mm laser beam spot diameter and 40% overlap recommended in recent studies [18,32] allowed us to obtain the adequate MCrAlY laser coatings evaluated in this work.

The mean thickness of the obtained NiCoCrAlY coating was 837 ± 26 µm. The BSE images (Fig. 3) revealed a dense coating with a homogeneous structure and minimal dilution with the austenitic stainless steel substrate (less than 2 µm). The microstructure morphology and elementary chemical analysis performed by EDS revealed two main phases: a matrix of γ-phase and a disperse β-phase. However, the measured thickness of the CoNiCrAlY alloy was slightly lower, 713 ± 33 µm under the same process parameters. The microstructure was revealed as a cellular dendritic structure. The BSE images together with the EDS microanalysis (Fig. 3) showed a dendritic γ–Ni matrix phase (bright zones) with the presence of Cr and Co elements in a solid solution form. Furthermore, an interdendritic β-NiAl phase

(dark zones) was also detected. Y-rich zones (bright zones) are present in some γ/β and γ/γ grain boundaries in both coatings (Figs. 3 and 4).

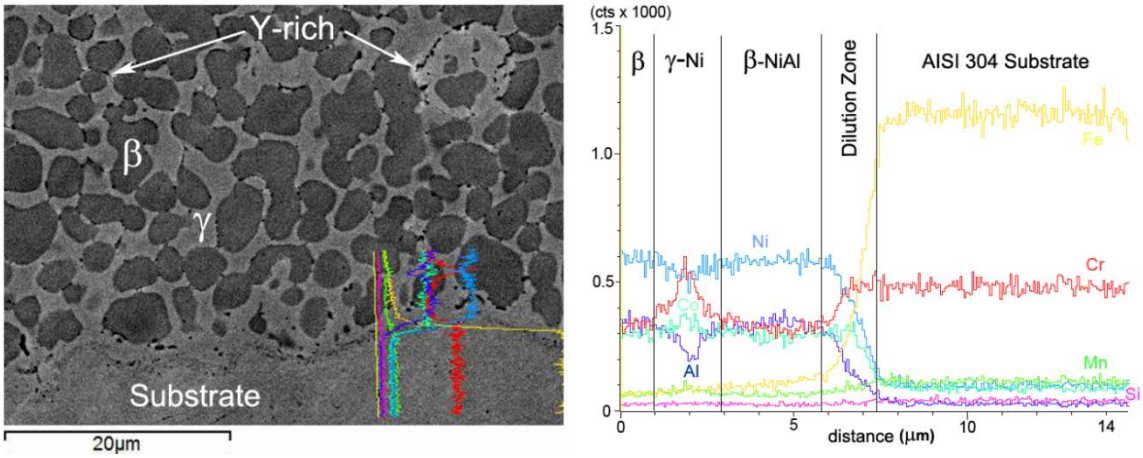

Fig. 3 SEM micrograph (2500X, 20 kV BSE mode) of the NiCoCrAlY laser coating, dilution and substrate zones; to the right, linescan of chemical composition at the interface

In the CoNiCrAlY coating, a columnar dendritic structure with a planar solidification front was observed (Fig. 4). In this case, the interdendritic phase (dark zone) is shorter than in the nickel-based coating due to the lower Al content in this alloy. The EDS analysis also suggests a hypoeutectic solidification with γ-Co(Ni,Cr) and β-(Co,Ni)Al interdendritic phase. The γ/β laser cladding coatings' microstructures were confirmed by DRX analysis (Fig. 5): the gamma phase crystal is cubic FCC (Fm3m, space group number 225), and the beta phase is cubic BCC (Pm-3m, space group number 221) [33].

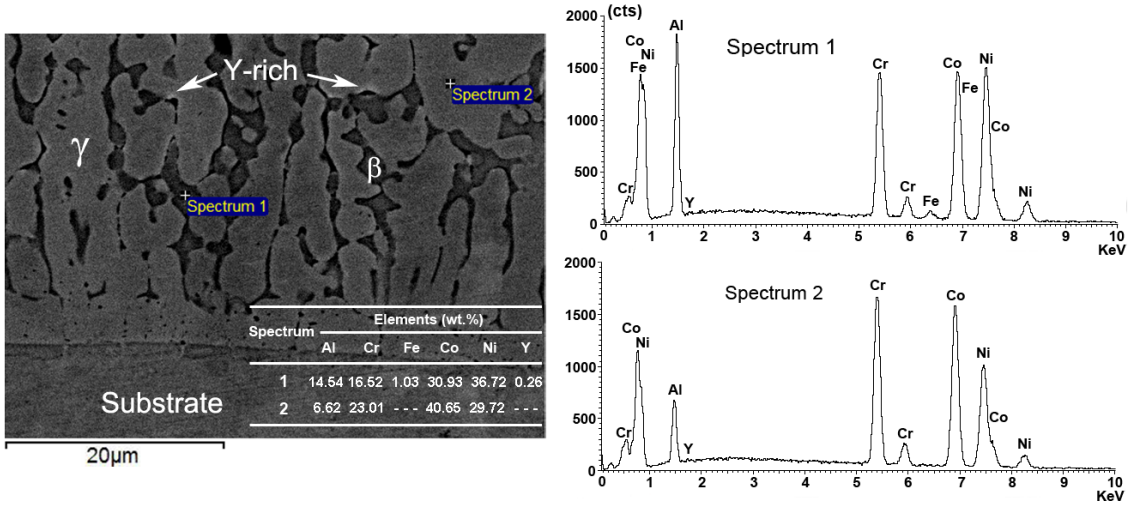

Fig. 4 SEM micrograph (2500X, 20 kV BSE mode) of the CoNiCrAlY laser coating area close to the interface with the substrate; on the right, chemical composition spectra with quantification of the elements present in the two main phases

The primary solidification phase is γ-dendrites, while the β-phase is formed in the interdendritic regions by the residual eutectic reaction at the end of the solidification and solid state precipitation. Nucleation is avoided, and the oriented cellular γ-dendrites are observed in the laser cladding coatings with the same orientation (vertical growth direction). Several Y-rich zones (bright white) were present in some γ/γ and γ/β grain boundaries; these results show and confirm that the yttrium-rich zones are randomly distributed, but always towards the grain boundaries or around porosities in both coatings. The *Marangoni effect* [18] was observed as changes in the morphology and direction of dendritic growth in the microstructure, due to the gradient of the cooling rates in depth.

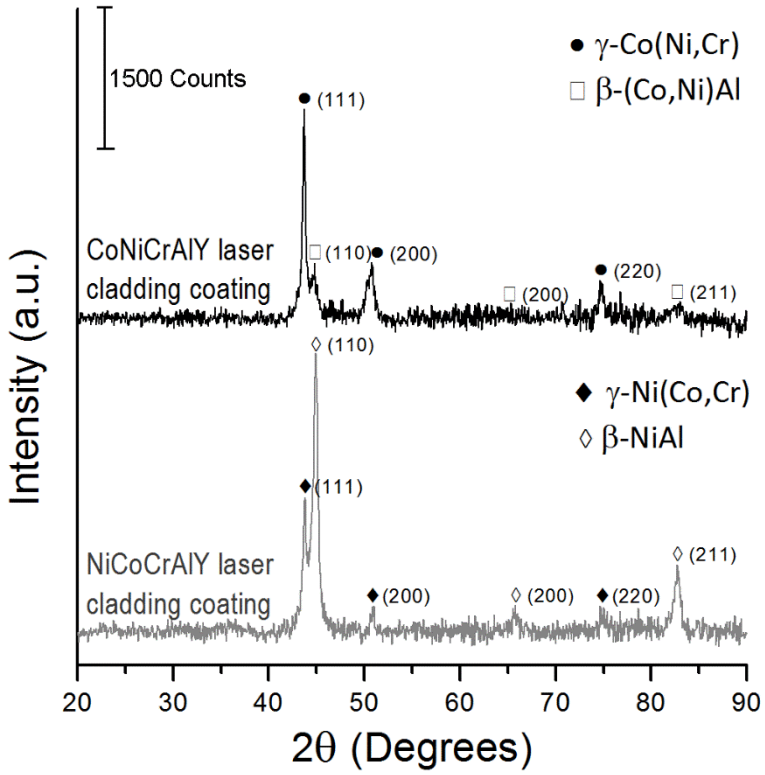

Fig. 5 XRD patterns acquired on the surface of both MCrAlY laser coatings and the two main crystallographic phases indexed

The dilution and mixing of relevant chemical elements such as Fe, Co, Al and Y with Ni-Cr from the surface of the coating to the substrate showed a gradual variation of composition influenced by the microstructure obtained. At a higher iron content in the solid solution

formed during the solidification in the area near the substrate, a lower hardness is obtained, as it is measured near the dilution zone, while a higher Al content increases the hardness, since this element stabilizes the β-phase, which is harder than the γ-phase [10,34]. The amount of β-phase detected at different zones of the coatings is double the γ-phase content in NiCoCrAlY with respect to CoNiCrAlY, representing 2/3 of the total composition. In the case of the CoNiCrAlY coating (Fig. 6), this proportion only represents about 1/4 due to the Al content of this alloy (12.5 wt.% versus the 8 wt.%, respectively). This observation verifies that the aluminum stabilizes the β-phase when MCrAlY coatings are obtained by laser cladding. Furthermore, in the interdendritic spaces at the end of the rapid solidification process, an Al content above the possible eutectic composition allows greater beta-phase formation, specifically in the NiCoCrAlY alloy with its higher aluminum content, which also influences the high-temperature oxidation behavior in this coating, as reported in previous work [35].

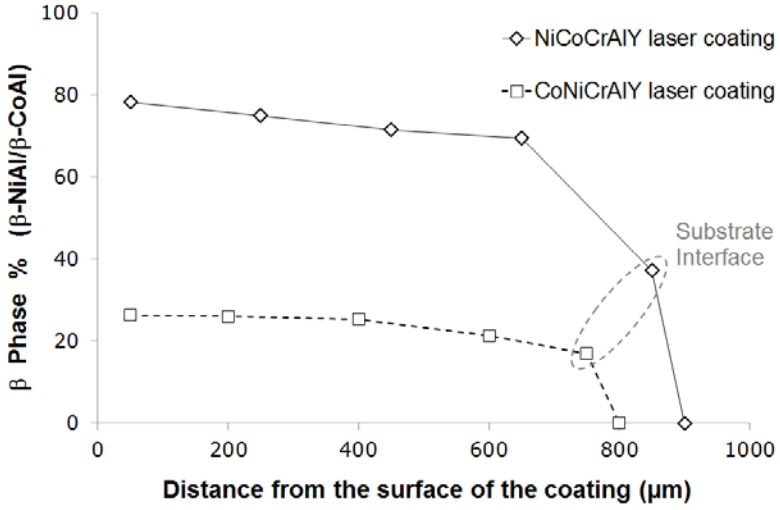

Fig. 6 Evolution of β-phase amount from the surface to substrate in the obtained γ/β MCrAlY laser coatings

3.2 Hardness profile

The mechanical resistance and durability of a TBC depends of the mechanical characteristics of each individual layer, the substrate characteristics and their relationship. In order to improve the resistance of the system, the coating's hardness must be greater than the substrate hardness

[31,36]. Moreover, a gradual gradient in substrate hardness in the interface region is desirable. That is why, in this initial section, we study the microhardness profile in the obtained laser coatings. The microhardness profiles obtained for both compositions are plotted in Figure 7. The average microhardness for NiCoCrAlY and CoNiCrAlY coatings was 492±13 HV and 361±15 HV, respectively, whereas the hardness for the stainless steel substrate was 234±10 HV, corroborating the higher H values desired for the coating. These results also demonstrate that the microhardness behavior along the coatings are quite constant. The observed H deviation in certain regions was expected due to the dendritic to columnar transition and due to the rich β-phase content in the interdendritic zones. Otherwise, the higher H values found in the NiCoCrAlY coating can be explained by the effect of the aluminum in the formed microstructure; that is, the NiCoCrAlY alloy has a greater amount of Al (12.5%wt) than the CoNiCrAlY alloy (8%wt), which modifies the microstructure by stabilizing the β-phase, as described previously.

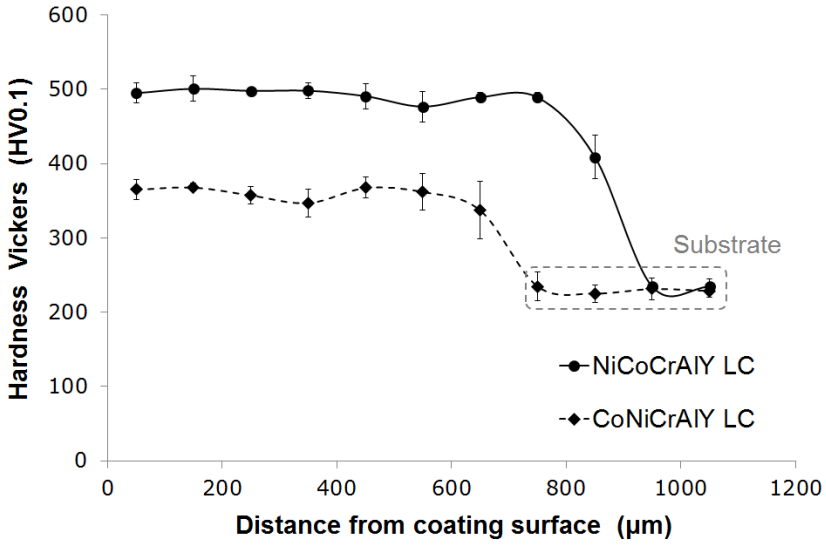

Fig. 7 Microhardness profile in MCrAlY laser coatings

It has been demonstrated that the hardness acquired for the NiCoCrAlY coating was higher than that reported for the conventional plasma spray and HVOF processes (Table 1). However, the hardness of the CoNiCrAlY coating resulted in a slightly lower H. Nevertheless, the overall

quality of both LC coatings studied was enhanced by the obtained microstructure without observable pores, defects or oxidized particles/material with these MCrAlY alloys. The improved microstructure obtained through LC should increase the coating's durability when compared with conventional thermal spray coatings.

Table 1. Comparative table of microhardness values in MCrAlY coatings obtained by coaxial laser cladding and thermal spray processes

Coating Material	Process	Microhardness (Kg/mm^2)	HV scale	Reference
NiCoCrAlY	Coaxial Laser Cladding	492 ± 13	$HV_{0.1}$	Own measurements
	HVOF	434 ± 64	$HV_{0.1}$	Mercier *et al* [37]
	Plasma spray	450 ± 45	$HV_{0.1}$	Brodin *et al* [38]
CoNiCrAlY	Coaxial Laser Cladding	361 ± 15	$HV_{0.1}$	Own measurements
	HVOF	410 ± 35	$HV_{0.3}$	Scrivani *et al* [39]
	Plasma spray	155 ± 18	$HV_{0.3}$	Higuera *et al* [40]

3.3 Elastic modulus and nanohardness

The microhardness analysis revealed that the β-phase stabilization effect from the aluminum leads to a harder coating. This hypothesis was clarified by analyzing the individual phases by nanoindentation tests on coating cross-sections. Figure 8 shows the in-depth H and E curves obtained for the NiCoCrAlY (Fig. 8a) and CoNiCrAlY (Fig. 8b) coatings. These curves evidence several characteristics to be considered: at low indentation depths (below 100nm deep), results are useless due to their highly scattered values. This phenomenon is explained by the roughness of the sample and by the pure elastic deformation mechanism produced at very low loads [41,42]. However, two well-defined tendencies were observed over the 100-750 nm depth range.

The range of depth marked in the figure has been used to calculate the H and E of each of the coating's individual phases. These values were subsequently assigned to γ- and β-phases by observing the location of each imprint made using FESEM. At the maximum indentation depth,

the curves converge due to the rule of mixtures [43,44], and these values were considered as those of the whole coating. A further analysis of the individual phases is described below, although an initial inspection of these curves reveals that the H and E values for each phase were inverted between them.

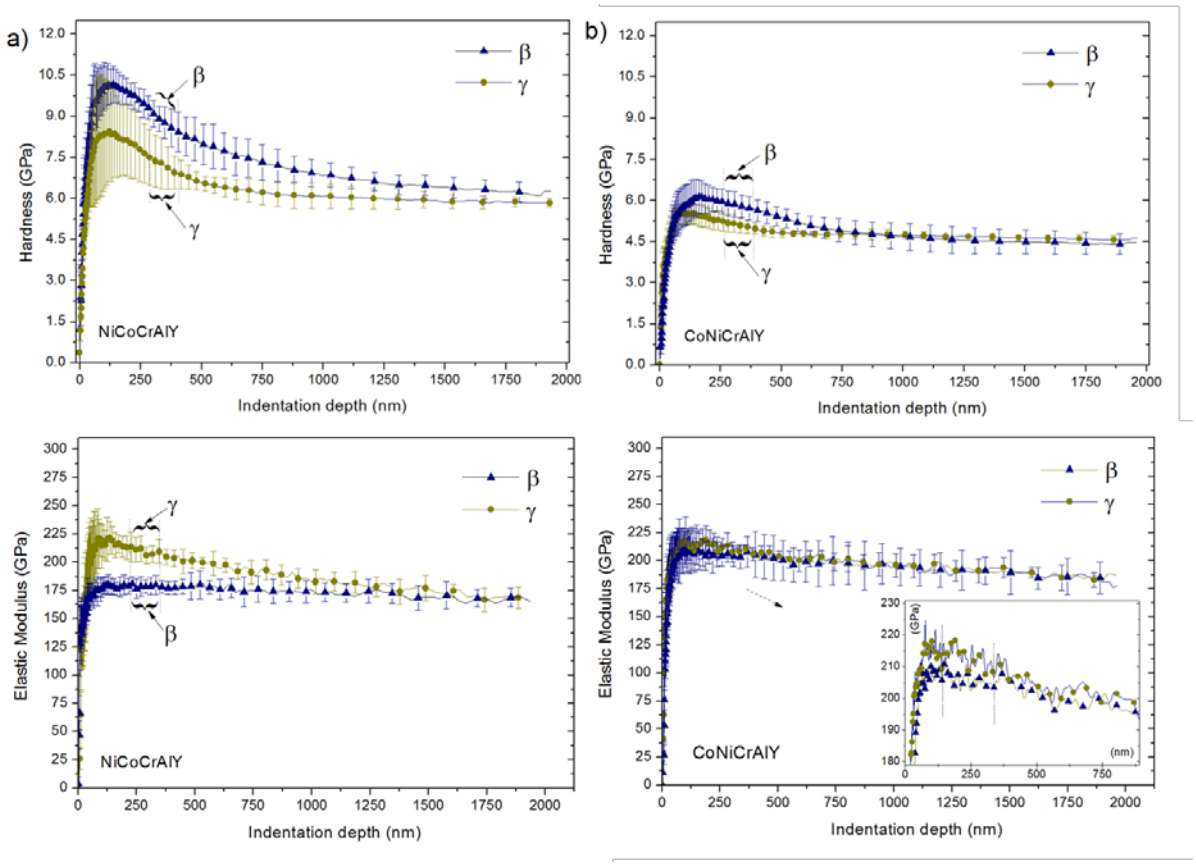

Fig. 8 In-depth Hardness and Elastic modulus curves obtained by nanoindentation for **a)** NiCoCrAlY coating and **b)** CoNiCrAlY coating.

The H and E values for each identified γ/β phase were calculated from the curves shown in Fig. 8 and summarized in Table 2. These results reveal an elastic modulus value for the whole NiCoCrAlY coating of 175±3 GPa, and of 191±3 GPa for the CoNiCrAlY coating. These E values were slightly lower than those obtained from the stainless used as substrate (240.9±7.3 GPa). The hardness was 6.2 GPa and 4.5 GPa for NiCoCrAlY and CoNiCrAlY coatings, corroborating the microhardness results. These characteristics suggest that failures such as delamination or detachment of the coating must be reduced, and are in agreement with previously reported values [22].

Table 2. Summary of the elastic modulus and hardness values calculated for each single phase identified in coatings.

Sample	Phase	Elastic Modulus (GPa)	Hardness (GPa)
NiCoCrAlY	γ-Ni	215.4 ± 9.7	7.5 ± 0.7
	β-NiAl	178.7 ± 6.8	9.7 ± 0.4
	Coating	175.5 ± 3.2	6.2 ± 0.1
CoNiCrAlY	γ-Co(Ni,Cr)	214.7 ± 10.9	5.3 ± 0.3
	β-(Co,Ni)Al	206.9 ± 13.	6.0 ± 0.5
	Coating	191.0 ± 3.4	4.5 ± 0.1

The elastic modulus of the γ-phases (215 GPa and 214 GPa) were higher than the β-phases (178 GPa and 206 GPa) for the NiCoCrAlY and CoNiCrAlY, respectively. Additionally, the hardness results followed an inverse trend to elastic moduli. The γ-phases reveal a lower hardness (7.5 GPa and 5.3 GPa) than the β-phases (9.7 GPa and 6.0 GPa) for NiCoCrAlY and CoNiCrAlY, respectively. The differences found for each given phase is due to both coatings having similar crystallography but different chemical composition; for example, there is a greater proportion of Ni-Cr solid solution elements in the NiCoCrAlY coating, leading to this phase hardening. The lower elastic modulus found in the γ-Ni phase is greater than that of the β-NiAl phase due to the type of elements in the solid solution (Co and Cr) instead of the intermetallic compounds in the aluminum-rich phase. However, the hardness of the β-NiAl phase is greater than in γ-Ni due to the higher percentage of the stabilized β-phase. These conclusions are in agreement with the results of previous studies on coatings performed by Low Vacuum Plasma Spray [10,21] and by conventional and sintered powder metallurgy [34] with similar alloys.

In conclusion, the mechanical properties of the NiCoCrAlY laser coating are determined by the higher hardness and low modulus of the β-NiAl phase, as we can see in Fig 9. For this coating, the highest difference was observed between the properties of the γ/β phases, and this characteristic could affect failure resistance. In the CoNiCrAlY coating, the difference between

the mechanical properties of the phases is much smaller because the β-(Co,Ni)Al phase has a lower aluminum content than the β-NiAl phase. Others authors [21] have confirmed through nanoindentation measurement and analysis that β-(Co,Ni)Al is harder than the γ-Co(Ni,Cr) phase due to the γ-phase having a very low fraction of solid solution strengthening elements.

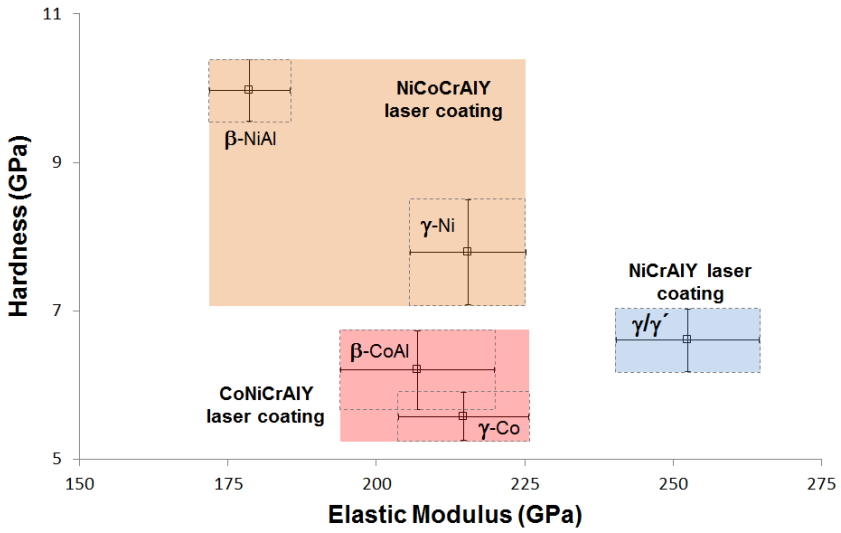

Fig. 9 Nanoindentation hardness & elastic modulus map for each individual phases in MCrAlY laser coatings. Results were calculated over the 100 to 300 nm depth range (own measurements)

3.4 Three-point bending tests

One of the simplest ways to evaluate mechanical strength in the coating-substrate assembly (and even the interface) is the three-point bending test. Flexural elastic properties have been obtained. Furthermore, the maximum resistance and the ductility of the coating were calculated until reaching catastrophic failure. The failure zone has also been analyzed by means of FESEM to study the failure mechanism both in the coating and in the coating-substrate interface zone. Fig. 10 shows the stress-strain curve of the coatings tested, both in longitudinal (Fig. 10a) and transverse orientation (Fig. 10b) with respect to the laser tracks overlap direction. The events that occurred during the test were detected by the abrupt deflection event using the extensometer, indicating the load at which the coating reached failure.

As observed in the bending stress vs. deformation curves, all the coatings failed in the plastic zone, so the ductility of the coatings is adequate to maintain their integrity in the elastic range; with the stress and deformation after the yield zone, coating failure occurs. Greater resistance has been obtained in the longitudinal direction of bending samples (Fig. 10a), and in the transverse samples, resistance and ductility are reduced. This behavior will be analyzed with electron microscopy images of the interface area (lateral view) in the coatings after the bending tests. The calculated values of the elastic modulus in bending, yield strength, failure stress and deformation for coating failure are listed in Table 3.

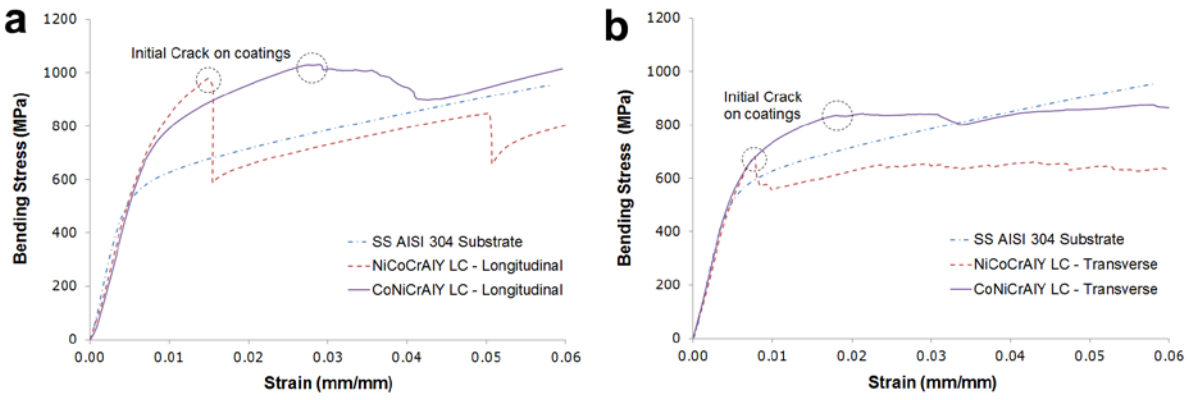

Fig. 10 Characteristic Bending Stress vs. Deformation curves obtained from the three-point bending tests in **a)** longitudinal samples and **b)** transverse samples

As expected, the austenitic stainless steel substrate AISI 304 presents a high ductility in the three-point bending tests. No cracks were generated on the surface with maximum tensile stress. The behavior of the stress vs. deformation curve is very linear, both in the elastic zone and then in the plastic zone (Fig. 10 i.e.), which denotes a hardening by gradual deformation in the stainless steel after the yield zone. But this is not the case in the coatings; all laser coatings failed in the plastic zone, as shown in Figs. 10a and 10b, which is a positive result since it is guaranteed that they will have satisfactory mechanical behavior in service (mechanical components are commonly designed to work in the elastic range). The bending yield stress of the MCrAlY coatings is higher than the substrate. Otherwise, the highest values observed in the

bending elastic modulus was recorded for the CoNiCrAlY alloy (in transverse samples), and the lowest values for the elastic modulus were obtained for the NiCoCrAlY coating (in longitudinal samples), which is in line with the trend observed in elastic modulus nanoindentation measurements.

Table 3. Three-point bending tests results

Material / Coating	Orientation of tracks in bending samples	Bending Elastic Modulus (GPa)	Bending Yield Strength (MPa)	Failure Strength (MPa)	Deformation at failure (%)
SS AISI 304	---	146.31 ± 4.11	546.83 ± 50.16	---	---
NiCoCrAlY	Longitudinal	118.29 ± 11.66	702.24 ± 98.81	902.59 ± 70.84	1.24 ± 0.28
	Transverse	123.19 ± 4.41	612.30 ± 91.57	766.60 ± 99.15	0.92 ± 0.27
CoNiCrAlY	Longitudinal	125.46 ± 7.94	731.67 ± 47.61	1029.61 ± 6.97	3.41 ± 0.53
	Transverse	136.30 ± 13.15	730.33 ± 54.28	840.85 ± 27.87	1.51 ± 0.42

A notable anisotropy characteristic was found in the case of the NiCoCrAlY coating. This coating presents the highest hardness, according to microhardness and nanoindentation measurements, although the bending elastic modulus is maintained constant in both orientations, in addition to a significant reduction of the bending yield strength (12.8% or 90 MPa) and strength at failure (15.07% or 136 MPa) in the transverse orientation. This effect indicates that when laser tracks are arranged in the transverse direction, a greater number of overlapping tracks, with more interface between them, are achieved. The ductility is reduced in the transverse orientation, and the resistance of the coating/substrate assembly in the plastic zone is also reduced, until reaching coating failure.

To analyze the failure mechanism of the coatings in both orientations, we can observe and compare the FESEM images on the lateral side of the tested samples (Figs. 12 and 13), where it is evident that, for NiCoCrAlY laser coatings, both orientations (longitudinal and transverse) present a failure mechanism by localized delamination (Fig. 12). In the case of the longitudinal

sample, it is observed that the coating is plastically deformed before failure, and there is a smaller delamination zone (Fig. 11a) than that observed in transverse sample (Fig. 11b), in which there is no plastic deformation of the coating (fragile-elastic behavior), which denotes a greater fragility (or brittle behavior) of the coating in this condition.

No internal cracks are observed in the cross section of both coatings, although at the end of the delamination zone in the interface with the substrate, small cracks are generated in the interface with the substrate (Figs. 11c and 11d). This behavior has been reported by other authors in NiCrAlY coatings after three-point bending tests in vacuum heat treated (annealed) samples, indicating that the crack nucleates and propagates along the interface, leading to the rupture of the brittle overlayer [23].

The failure zone of the NiCoCrAlY coating in the longitudinal orientation has a higher crack density than that observed in the transverse orientation, where failure was catastrophic due to a vertical crack. The fragility is associated with the high hardness of the coating as previously measured by microhardness and nanoindentation tests, while the failure by delamination is due to the notable difference in the elastic modulus between both materials, as well as the high ductility of the substrate and the fragility that the NiCoCrAlY coating presents, based on the fact that an adequate metallurgical bonding was achieved between both materials as well as a low dilution of the chemical elements of the substrate.

The way in which the coating failed internally can be closely associated with the dendritic microstructure of the coating, since the great difference between elastic modulus and hardness presented by the γ- and β-phases that constitute its microstructure can favor intergranular fracture in the dendritic area, although this aspect was not studied in detail on the failure surfaces since the test was stopped at 6% of total deformation.

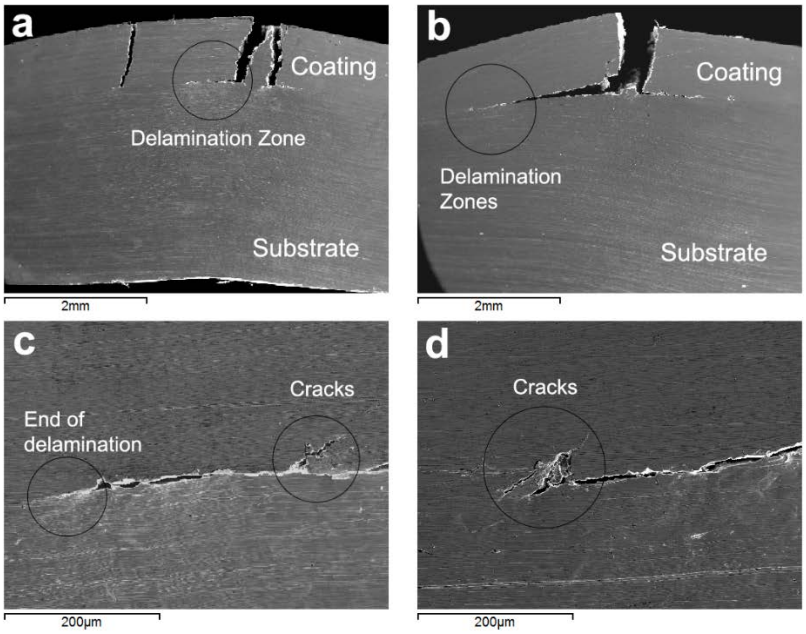

Fig. 11 SEM micrographs (20 kV SE mode) of the NiCoCrAlY coating after the bending tests: **a)** longitudinal sample **b)** transverse sample **c)** cracks in longitudinal sample and **d)** cracks in transverse sample

The CoNiCrAlY coating did not show delamination, and failure is due to vertical cracks that nucleate in the area of highest tension (outer fiber of the coating) and propagate to the interface. In the case of the longitudinal sample, a single crack is generated (Fig. 12a), while in the transverse sample, at least four cracks are observed (Fig. 12b). There is a slight increase in the elastic limit in comparison with the NiCoCrAlY coating, and it is higher than the substrate (good correspondence of the coatings in the elastic zone). Resistance is significantly reduced until failure in the transverse orientation (18.3% or 188.76 MPa), with an increase of the elastic modulus of 8.6% or 10.8 GPa.

The highest resistance was achieved in longitudinal samples of CoNiCrAlY coating due to the excellent metallurgical bond with the substrate which is evident in the absence of delamination in the interface zone (Fig. 12c), and due to its high ductility. Although there is also excellent metallurgical bonding in the transverse orientation, multiple vertical cracks are generated (Fig. 12d) only in the coating material, some of which do not reach the external surface of the coating, showing cracks separated from each other but which start from the coating/coating interface

(Fig. 13d). This failure behavior is much better than the delamination and multiple cracks reported in HVOF CoNiCrAlY coatings on Ti6Al4V when subjected to three point bending tests [45].

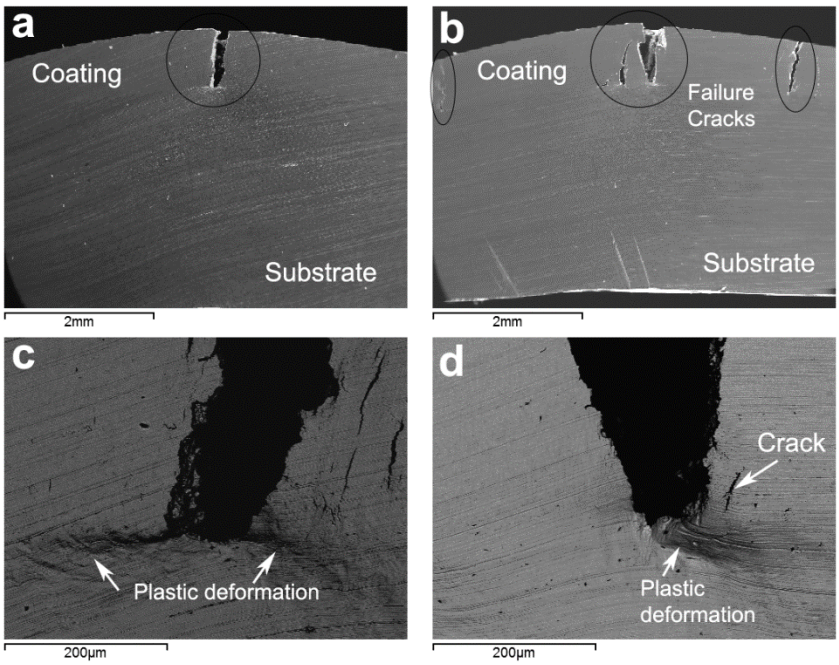

Fig. 12 SEM micrographs (20 kV) of the CoNiCrAlY coating after the bending test: **a)** longitudinal sample (SE mode) **b)** transverse sample (SE mode) **c)** failure detail in longitudinal sample (BSE mode) and **d)** failure detail area in transverse sample (BSE mode)

In the high-magnification micrographs of the failure zone, it can be observed how both orientations in the coating and the substrate have been plastically deformed in a similar way until reaching coating failure (Figs. 12a to 12c), associated with the low hardness of the γ-(Co,Ni)Cr matrix which gives it a high ductility, so it can be asserted that the failure mechanism is exclusively through nucleation of cracks in the coating. Around the main crack, micro cracks parallel to this can be observed and suggest the nucleation of cracks from the interface in the areas between overlapping laser tracks, since this it is where changes in the orientation of the solidification are found, favoring accumulation of nucleation.

If the results obtained in the CoNiCrAlY coating are compared with those reported in similar bond coats obtained by plasma spray [10,46], it is observed that the resistances reached in bending in the laser coatings are double the values measured in a three-point bending test both

for the yield strength and for the maximum resistance until coating failure. The anisotropy in the mechanical properties obtained from this test depend on the amount of interface between the overlapping laser tracks. As a common factor, there is a greater amount of lacing interface in the tracks arranged with transverse orientation, which increases not only the defects associated with them, but also increases the possibility of failure due to intergranular cracks in the dendritic areas. The solidification direction changes and chemical composition of the phases also have an affect, in addition to a lower homogeneity in the metallurgical bond of each laser track (15 in total) with the substrate, since each pass has a separate heat accumulation of the heat input generated by the laser energy density.

The study of the mechanical behavior of the obtained laser coatings and the extreme correlation with their microstructure in as-built condition allow us to provide to the scientific community with greater knowledge of the mechanical properties that can be obtained with laser processing of MCrAlY alloys. In this work, we have focused on obtaining bond coats through LC, and in the future, this could be used for the manufacture of components by LMD.

4. Conclusions

Dense MCrAlY coatings exhibiting adequate metallurgical bonding with the substrate were obtained by overlapping coaxial laser cladding; the microstructure is composed mainly of a γ-(Ni,Co)Cr matrix phase and a β-(Ni,Co)Al interdendritic phase, confirmed by XRD, with some Y-rich areas around grain boundaries or small pores.

The MCrAlY laser coatings have a higher microhardness than the AISI 304 stainless steel substrate. The hardness of the main phases that make up the coatings has been measured by nanoindentation. The β-phase rich in aluminum was harder than the γ-phase, so in MCrAlY laser coatings with γ/β microstructure, the hardness may be higher than in γ/γ' coatings.

The mechanical properties measured by nanoindentation tests make it possible to assert that the γ/β MCrAlY laser coatings have elastic modulus and hardness similar to those reported in

conventional thermal projection processes, but with a microstructure characteristic of a fusion process, with rapid solidification outside the balance, a lower level of porosity and no defects. The elastic modulus of the NiCoCrAlY and CoNiCrAlY coatings were lower than the substrate; this property has behavior that is inversely proportional to the hardness of the laser coating, so that a greater amount of β-(Ni,Co)Al phase, lower elastic modulus and lower ductility are obtained in laser coatings with γ/β microstructure.

The obtained MCrAlY laser coatings showed good performance in the three-point bending tests; all coatings failed in the plastic range, with a failure resistance higher than the elastic limit of the substrate. The lowest resistance was for the NiCoCrAlY coating, which presented an elastic-fragile behavior, with a failure mechanism by delamination and cracks from the interface with the substrate. The highest resistance was for the CoNiCrAlY coating, which presented an elastic-plastic behavior, crack failure without any delamination and high ductility.

There was an anisotropy feature in the flexural behavior according to the deposition direction of the overlapping laser tracks, significantly reducing the resistance in the transverse orientation. The anisotropy was explained due to a greater number of lacing interfaces, favoring intergranular fracture in the dendritic areas with sudden changes in the solidification direction, in addition to less homogeneity in the metallurgical connection of the tracks with the substrate.

The results confirmed that coaxial laser cladding is a good alternative to the thermal spray process to obtain a good quality bond coat, and that MCrAlY laser coatings show adequate mechanical properties in terms of elastic modulus, hardness and ductility for use in TBC systems, and offer a promising outlook for future additive manufacturing using LMD with MCrAlY alloys.

5. Acknowledgments

The authors would like to acknowledge the financial support of the Ministry of Science and Innovation of the Government of Spain through research project MAT2011-28492-C03, and the support of the Generalitat Valenciana through ACOMP/2013/114.

References

[1] X.Q. Cao, R. Vassen, D. Stoever, Ceramic materials for thermal barrier coatings, J. Eur. Ceram. Soc. 24 (2004) 1–10. doi:10.1016/S0955-2219(03)00129-8.

[2] N.P. Padture, M. Gell, E.H. Jordan, Thermal Barrier Coatings for Gas-Turbine Engine Applications, Science (80-.). 296 (2002) 280–284. doi:10.1126/science.1068609.

[3] B.A. Pint, J.A. Haynes, Y. Zhang, Effect of superalloy substrate and bond coating on TBC lifetime, Surf. Coatings Technol. 205 (2010) 1236–1240. doi:10.1016/j.surfcoat.2010.08.154.

[4] P. Carpio, E. Rayón, M.D. Salvador, L. Lusvarghi, E. Sánchez, Mechanical Properties of Double-Layer and Graded Composite Coatings of YSZ Obtained by Atmospheric Plasma Spraying, J. Therm. Spray Technol. 25 (2016) 778–787. doi:10.1007/s11666-016-0390-z.

[5] U. Schulz, C. Leyens, K. Fritscher, M. Peters, B. Saruhan-Brings, O. Lavigne, J.M. Dorvaux, M. Poulain, R. Mévrel, M. Caliez, Some recent trends in research and technology of advanced thermal barrier coatings, Aerosp. Sci. Technol. 7 (2003) 73–80. doi:10.1016/S1270-9638(02)00003-2.

[6] M.J. Pomeroy, Coatings for gas turbine materials and long term stability issues, Mater. Des. 26 (2005) 223–231. doi:10.1016/j.matdes.2004.02.005.

[7] F. Tancret, H.K.D.H. Bhadeshia, D.J.C. MacKay, Design of a creep resistant nickel base superalloy for power plant applications: Part 1 - Mechanical properties modelling, Mater. Sci. Technol. 19 (2003) 283–290. doi:10.1179/026708303225009788.

[8] T.J. Nijdam, C. Kwakernaak, W.G. Sloof, The effects of alloy microstructure refinement on the short-term thermal oxidation of NiCoCrAlY alloys, Metall. Mater. Trans. A. 37 (2006) 683–693. doi:10.1007/s11661-006-0040-z.

[9] G. Marginean, D. Utu, Cyclic oxidation behaviour of different treated CoNiCrAlY coatings, Appl. Surf. Sci. 258 (2012) 8307–8311. doi:10.1016/j.apsusc.2012.05.050.

[10] D.-J. Kim, S.-K. Cho, J.-H. Choi, J.-M. Koo, C.-S. Seok, M.-Y. Kim, Evaluation of the Degradation of Plasma Sprayed Thermal Barrier Coatings Using Nano-Indentation, J. Nanosci. Nanotechnol. 9 (2009) 7271–7277. doi:10.1166/jnn.2009.1786.

[11] J. De Damborenea, A.J. Vázquez, Laser cladding of high-temperature coatings, J. Mater. Sci. 28 (1993) 4775–4780. doi:10.1007/BF00414271.

[12] R. Vilar, Laser cladding, J. Laser Appl. 11 (1999) 64–79. doi:10.2351/1.521888.

[13] A. Segerstark, J. Andersson, L.-E. Svensson, Investigation of laser metal deposited Alloy 718 onto an EN 1.4401 stainless steel substrate, Opt. Laser Technol. 97 (2017) 144–153. doi:10.1016/j.optlastec.2017.05.038.

[14] A. Singh, A. Ramakrishnan, G.P. Dinda, Direct Laser Metal Deposition of Eutectic Al-Si Alloy for Automotive Applications, in: M.& M.S. TMS The Minerals (Ed.), TMS 2017 146th Annu. Meet. Exhib. Suppl. Proc., Springer International Publishing, Cham, 2017: pp. 71–80. doi:10.1007/978-3-319-51493-2_8.

[15] R.M. Mahamood, Laser Metal Deposition of Metals and Alloys, in: Laser Met. Depos. Process Met. Alloy. Compos. Mater., Springer International Publishing, Cham, 2018: pp. 93–118. doi:10.1007/978-3-319-64985-6_5.

[16] D. Texier, D. Monceau, F. Crabos, E. Andrieu, Tensile properties of a non-line-of-sight processed β-γ-γ′ MCrAlY coating at high temperature, Surf. Coatings Technol. 326 (2017) 28–36. doi:10.1016/j.surfcoat.2017.07.026.

[17] F. Vollertsen, K. Partes, J. Meijer, State of the Art of Laser Hardening and Cladding, in: E. Beyer, F. Dausinger, A. Ostendorf, A. Otto (Eds.), Proc. Third Int. WLT-Conference Lasers Manuf. 14-17 June 2005, Munich, Ger., AT-Fachverlag GmbH, 2005: pp. 281–305.

[18] J.D. Majumdar, I. Manna, Laser material processing, Int. Mater. Rev. 56 (2011) 341–388. doi:10.1179/1743280411Y.0000000003.

[19] D. Texier, D. Monceau, Z. Hervier, E. Andrieu, Effect of interdiffusion on mechanical and thermal expansion properties at high temperature of a MCrAlY coated Ni-based superalloy, Surf. Coatings Technol. 307 (2016) 81–90. doi:10.1016/j.surfcoat.2016.08.059.

[20] X. Zhao, Z. Xie, P. Munroe, Nanoindentation of hard multilayer coatings: Finite element modelling, Mater. Sci. Eng. A. 528 (2011) 1111–1116. doi:10.1016/j.msea.2010.09.073.

[21] R. Webler, M. Ziener, S. Neumeier, P.J. Terberger, R. Vaßen, M. Göken, Evolution of microstructure and mechanical properties of coated Co-base superalloys during heat treatment and thermal exposure, Mater. Sci. Eng. A. 628 (2015) 374–381. doi:10.1016/j.msea.2015.01.060.

[22] S. Saeidi, K.T. Voisey, D.G. McCartney, Mechanical Properties and Microstructure of VPS and HVOF CoNiCrAlY Coatings, J. Therm. Spray Technol. 20 (2011) 1231–1243. doi:10.1007/s11666-011-9666-5.

[23] W.Z. Li, Y. Yao, Y.Q. Li, J.B. Li, J. Gong, C. Sun, X. Jiang, Damage behavior of the NiCrAlY coating systems with or without barrier layer during three-point bending, Mater. Sci. Eng. A. 512 (2009) 117–125. doi:https://doi.org/10.1016/j.msea.2009.01.032.

[24] Z.X. Chen, Z.G. Wang, F.H. Yuan, S.J. Zhu, Interfacial fracture behavior of a thermal barrier coating system under four-point bend loading, Mater. Sci. Eng. A. 483–484 (2008) 629–632. doi:10.1016/j.msea.2007.01.166.

[25] D.W. Hetzner, Microindentation Hardness Testing of Materials Using ASTM E384,

Microsc. Microanal. 9 (2003) 708–709. doi:10.1017/s1431927603443547.

[26] W.C. Oliver, G.M. Pharr, Measurement of hardness and elastic modulus by instrumented indentation: Advances in understanding and refinements to methodology, J. Mater. Res. 19 (2004) 3–20. doi:10.1557/jmr.2004.19.1.3.

[27] J.J. Roa, M. Martínez, E. Rayón, N. Ferrer, F. Espiell, M. Segarra, Hardness of FRHC-Cu Determined by Statistical Analysis, J. Mater. Eng. Perform. 23 (2014) 637–642. doi:10.1007/s11665-013-0770-1.

[28] J.C. Pereira, J.J. Candel, J.M. Amado, V. Amigó, Geometric and microstructural analysis of laser clad NiCoCrAlYTa coating on stainless steel AISI 316L |Análisis geométrico y microestructural de recubrimientos de NiCoCrAlYTa proyectados por láser sobre láminas de acero inoxidable AISI 316L, Rev. Latinoam. Metal. Y Mater. 34 (2014) 209–2017. http://rlmm.org/ojs/index.php/rlmm/article/view/489.

[29] M.J. Tobar, J.M. Amado, A. Yáñez, J.C. Pereira, V. Amigó, Laser cladding of MCrAlY coatings on stainless steel, in: Phys. Procedia, 2014: pp. 276–283. doi:10.1016/j.phpro.2014.08.172.

[30] J.C. Pereira, J.C. Zambrano, M.J. Tobar, A. Yañez, V. Amigó, Desarrollo y caracterización de recubrimientos láser MCrAlY para aplicaciones de barrera térmica, Trater Press. 58 (2017) 30–39.

[31] J.C. Pereira, J.C. Zambrano, M.J. Tobar, A. Yañez, V. Amigó, High temperature oxidation behavior of laser cladding MCrAlY coatings on austenitic stainless steel, Surf. Coatings Technol. 270 (2015) 243–248. doi:10.1016/j.surfcoat.2015.02.050.

[32] V. Ocelík, O. Nenadl, A. Palavra, J.T.M. De Hosson, On the geometry of coating layers formed by overlap, Surf. Coatings Technol. 242 (2014) 54–61. doi:10.1016/j.surfcoat.2014.01.018.

[33] G.K. Dey, Physical metallurgy of nickel aluminides, Sadhana. 28 (2003) 247–262.

[34] J.C. Pereira, J.C. Zambrano, C.R.M. Afonso, V. Amigó, Microstructure and mechanical properties of NiCoCrAlYTa alloy processed by press and sintering route, Mater. Charact. 101 (2015) 159–165. doi:10.1016/j.matchar.2015.02.001.

[35] D. Kim, I. Shin, J. Koo, S. Kim, D. Seo, J. Kim, C. Seok, Quantitative analysis on the depletion rate of β-NiAl phases in MCrAlY coating, J. Mech. Sci. Technol. 28 (2014) 513–519. doi:10.1007/s12206-013-1118-3.

[36] J. Pereira, J. Zambrano, M. Licausi, M. Tobar, V. Amigó, Tribology and high temperature friction wear behavior of MCrAlY laser cladding coatings on stainless steel, Wear. 330 (2015) 280–287. doi:10.1016/j.wear.2015.01.048.

[37] D. Mercier, B.D. Gauntt, M. Brochu, Thermal stability and oxidation behavior of nanostructured NiCoCrAlY coatings, Surf. Coatings Technol. 205 (2011) 4162–4168. doi:10.1016/j.surfcoat.2011.03.005.

[38] H. Brodin, M. Eskner, The influence of oxidation on mechanical and fracture behaviour of an air plasma-sprayed NiCoCrAlY bondcoat, Surf. Coatings Technol. 187 (2004) 113–121. doi:10.1016/j.surfcoat.2003.12.021.

[39] A. Scrivani, U. Bardi, L. Carrafiello, A. Lavacchi, F. Niccolai, G. Rizzi, A comparative study of high velocity oxygen fuel, vacuum plasma spray, and axial plasma spray for the deposition of CoNiCrAlY bond coat alloy, J. Therm. Spray Technol. 12 (2003) 504–507. doi:10.1361/105996303772082242.

[40] V. Higuera, F.J. Belzunce, J. Riba, Influence of the thermal-spray procedure on the properties of a CoNiCrAlY coating, Surf. Coatings Technol. 200 (2006) 5550–5556. doi:10.1016/j.surfcoat.2005.07.070.

[41] J.J. Roa, E. Rayon, M. Morales, M. Segarra, Contact mechanics at nanometric scale using nanoindentation technique for brittle and ductile materials, Recent Pat. Nanotechnol. 6 (2012) 142—152. doi:10.2174/187221012800270162.

[42] G. Oncins, J.J. Roa, E. Rayón, J. Díaz, M. Morales, M. Segarra, F. Sanz, Friction, hardness and elastic modulus determined by AFM-FS and nanoindentation techniques for advanced ceramics materials, in: J.J. Roa Rovira, M. Segarra Rubi (Eds.), Recent Adv. Ceram. Mater. Res., Nova Science Publishers, 2013: pp. 215–250.

[43] R. Saha, W.D. Nix, Effects of the substrate on the determination of thin film mechanical properties by nanoindentation, Acta Mater. 50 (2002) 23–38. doi:10.1016/S1359-6454(01)00328-7.

[44] Y. Huang, F. Zhang, K.C. Hwang, W.D. Nix, G.M. Pharr, G. Feng, A model of size effects in nano-indentation, J. Mech. Phys. Solids. 54 (2006) 1668–1686. doi:10.1016/j.jmps.2006.02.002.

[45] D. Al-Anazi, M.S.J. Hashmi, B.S. Yilbas, Three-point bend testing of HVOF AMDRY 9954 coating on Ti–6Al–4V alloy, J. Mater. Process. Technol. 174 (2006) 204–210. doi:10.1016/j.jmatprotec.2005.11.038.

[46] H. Waki, A. Kobayashi, Influence of the mechanical properties of CoNiCrAlY under-coating on the high temperature fatigue life of YSZ thermal-barrier-coating system, Vacuum. 83 (2008) 171–174. doi:https://doi.org/10.1016/j.vacuum.2008.03.063.